PII: S1353-2561(01)00050-0

Prediction of the Dispersal of Oil Transport in the Caspian Sea Resulting from a Continuous Release

K.A. KOROTENKO†*, R.M. MAMEDOV‡, & C.N.K. MOOERS§, 2

†Shirshov Institute of Oceanology, Moscow, Russia

‡Institute Geography of Azerbaijan Academy of Sciences, 31 Javida, Baku 370143, Azerbaijan

§Rosensteel School of Marine and Atmospheric Sciences (RSMAS), University of Miami, 4600 Rickenbacker Csw, Miami 33149, USA

A 3-D hybrid flow/transport model has been developed to predict the dispersal of oil pollution in coastal waters. The transport module of the model takes predetermined current and turbulent diffusivities and uses Lagrangian tracking to predict the motion of individual particles (droplets), the sum of which constitute a hypothetical oil spill. Currents and turbulent diffusivities used in the model have been generated by a numerical ocean circulation model (Princeton ocean model) implemented for the Caspian Sea. The basic processes affecting the fate of the oil spill are taken into account and parameterized in the transport model.

The hybrid model is implemented for a simulated continuous release in the coastal waters of the Caspian Sea. The potential of the model for the prediction of the advective and turbulent transport and dispersal of oil spills is demonstrated. © 2001 Elsevier Science Ltd. All rights reserved.

Keywords: Caspian sea, oil spill, particle modelling

Introduction

"Petroleum companies from around the globe have descended on the independent countries that border the oil-rich Caspian Sea to develop new and old fields. They have signed contracts worth tens of billions of dollars in what is the century's last big oil bonanza." ³

Beyond "the benefits" such projects carry the certain threat to the marine environment in case of unconstrained development and transportation of oil and petroleum products. Thus, the creation of operational systems for the prediction of the transport and dispersal of oil pollutants in case of possible accidental spills are generally included during the development of oil fields.

The Caspian Sea (Fig. 1, left), extends zonally from 46.6 to 54.8 E and meridionally from 36.6 to 47.0 N. Over 60% of the Sea is shoaler than 100 m. There are two relatively deep basins (about 600 and 800 m, respectively) in the central and southern parts of the Sea. The shelf zone is very wide, and steep slopes occur only in the two deep basins. The Caspian Sea is an enclosed sea with major freshwater input from the Volga River balanced by evaporation, which the most concentrated in the Garabogazkol. The dynamics of the Caspian Sea are essentially those of mesoscale

^{*}Corresponding author. Present address: OCE URI, 217 Sheets Building, Narragansett, RI 02882, USA. Tel.: +1-401-874-6637; fax: +1-401-874-6837.

E-mail addresses: korotenko@oce.uri.edu (K.A. Korotenko), ramiz@lan.ab.az (R.M. Mamedov), cmooers@rsmas.miami.edu (C.N.K. Mooers).

¹ Tel.: +994-12-39-3541; fax: +994-12-97-5285.

² Tel.: +1-305-361-47; fax: +1-305-361-4797.

³ Steve LeVine. A cocktail of oil and politics. New York Times, November 19, 1999.

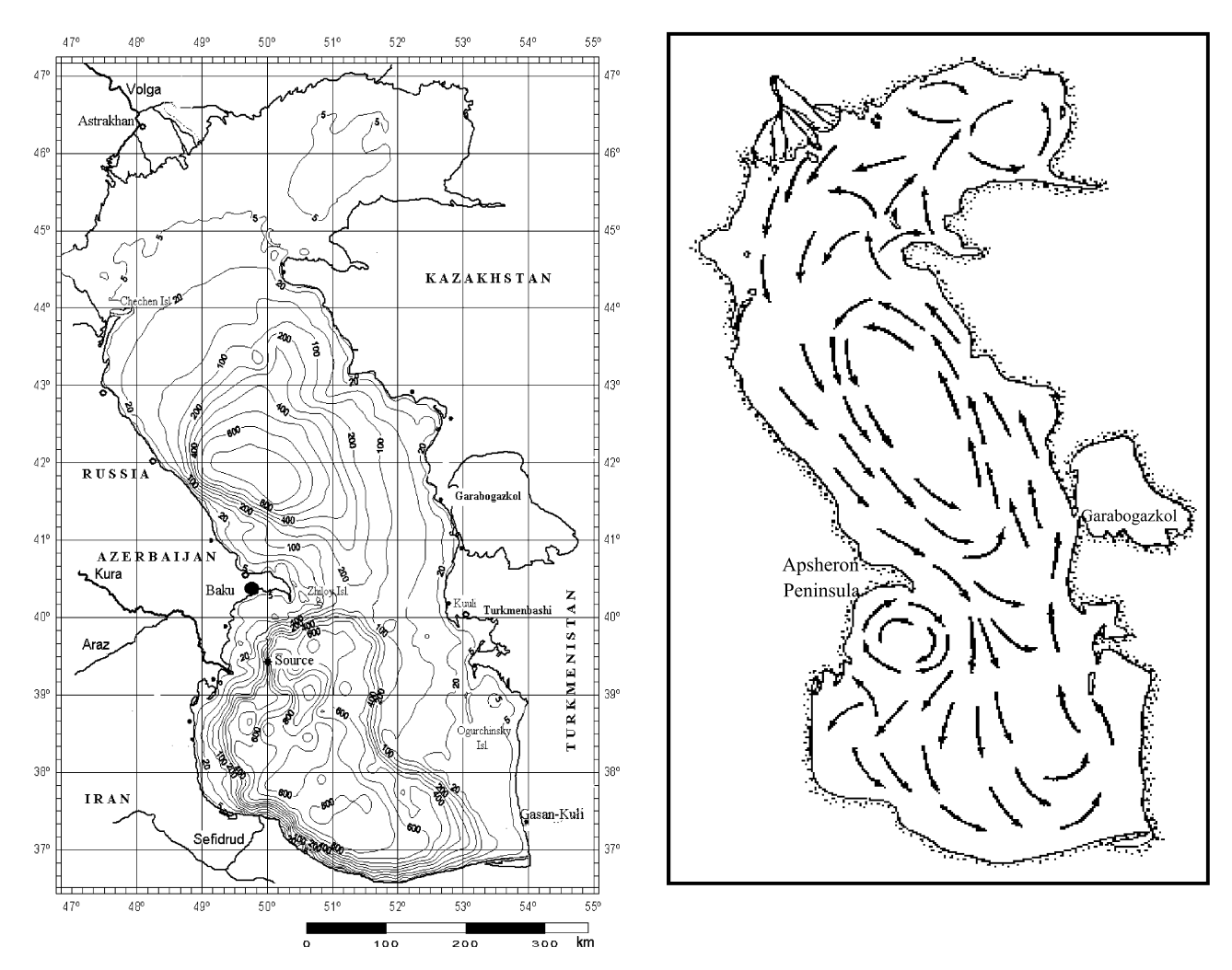


Fig. 1 The Caspian Sea (bottom topography (left) and sea circulation schematic (right)) (from Lednev, 1942).

space and time scales due to both mesoscale baroclinic motions and bottom topographic irregularities. A wide variety of processes in the Sea; e.g., interactions between shelf and deep basin circulation, deep basin ventilation, and ice dynamics. The nature of the air—sea interactions ranges from subtropical to subpolar types which constitutes an essential difference in dynamics between the meridionally oriented Caspian Sea and such zonally-oriented semi-enclosed seas as the Black and Baltic Seas.

In the Caspian Sea, salinity varies from zero in the shallow northern part (in vicinity of the Volga river discharge zone) to 14 ppt in the southeastern part. Furthermore, salinity generally increases with longitude and depth. Mean temperature has large meridional and seasonal variations of up to 27°C in summer and down to zero in winter. A relatively shallow seasonal thermocline occurs at depths of 10–40 m, and is absent in winter. Salinity and temperature in the bottom layer of the two deep basins are almost constant and average about 13 ppt, 4 C and 12 ppt, 6 C, respectively, for the central and southern basins. The

mean temperature, salinity, and density (sigma-t) distributions for the four seasons along 39° N (Fig. 2) illustrate the above features.

The "classical" mean circulation scheme in the Caspian Sea was proposed by Lednev (1943) (Fig. 1, right). Main features of the circulation are a cyclonic gyre over the central basin, jet-like current in the cyclonic sense along the western and eastern boundaries, and an anticyclinic gyre south of the Apsheron Peninsula. The meridional wind stress (in the winter directed southward) plays an important role and southward winds generate a southward drift current. In turn, a compensatory current is directed northward as a reaction to the elevated water level in the south. Due to the zonal inhomogeneity of wind stress (strong on western side and weak on the eastern side), the compensatory current intersects the surface along the eastern boundary creating a cyclonic circulation over the entire deep part of the Caspian Sea. The Apsheron Peninsula splits the southward current into two branches: the first branch is deflected to the east, and combines with the northward current along the



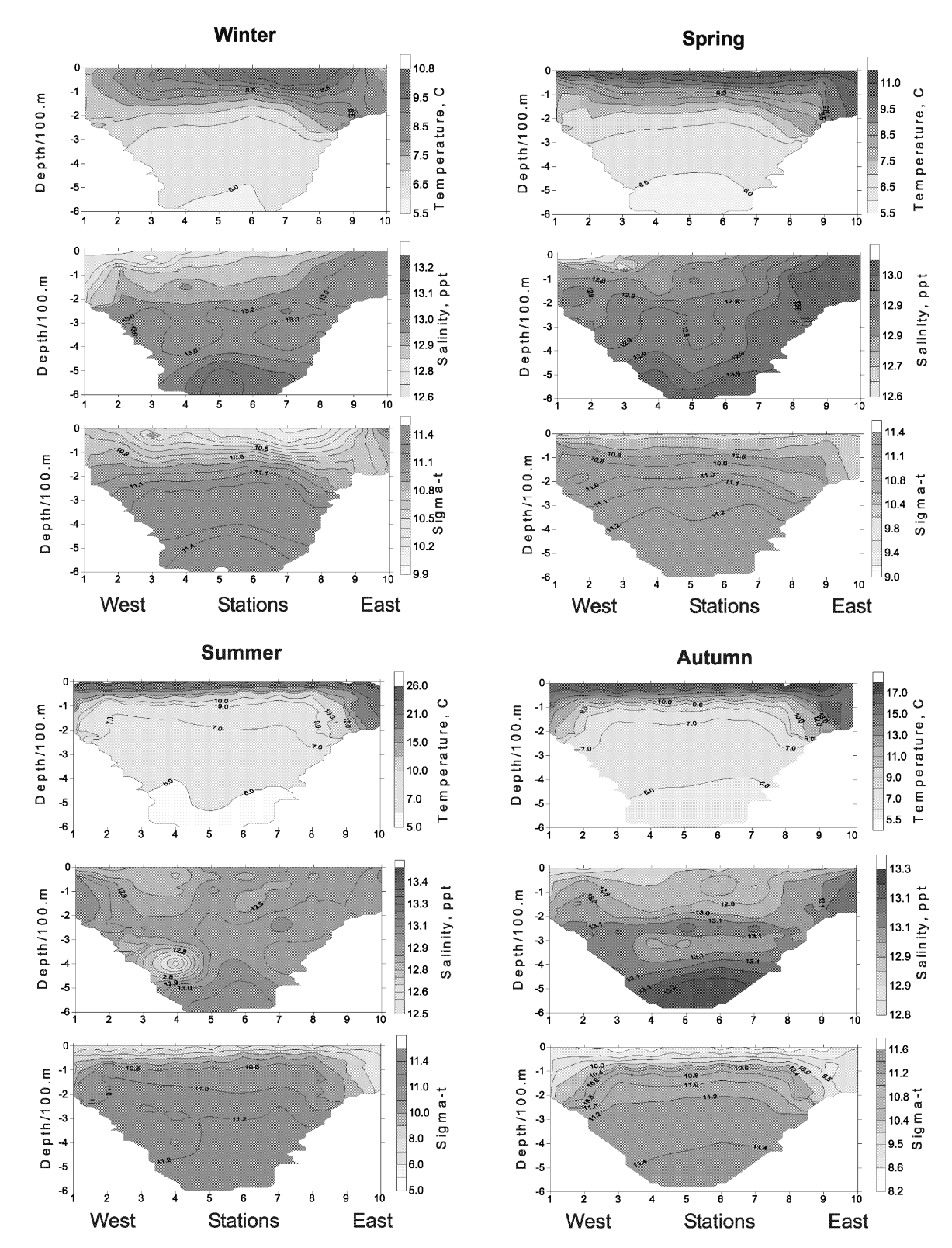


Fig. 2 Mean seasonal temperature, salinity, and cross-sections along 39° N.

eastern boundary, and thus, creates the closed cyclonic circulation (gyre) in the Central Caspian. The second branch of the current flows southward, and then along

the Iranian coast before being deflected to the north; thus, the closed the circulation in the Central Caspian is formed. An anticyclonic eddy, the so-called Kurine eddy (Fig. 1, right), occurs south of Apsheron Peninsula; however, its position might be different according to observations (Klevtsova, 1967; Kosarev, 1990; Bondarenko, 1993; Tuzhilkin et al., 1997). They have also shown that the "classical scheme" (Fig. 1, right) is a rather coarse approximation to reality; for example, strengthening of the southward winds intensifies the southward drift current on the eastern boundary, which dominates over the compensatory northward current at the surface and results in a southward surface flow at this boundary in contradiction to the "classical scheme". The southward jet is associated with upwelling along the eastern boundary, while downwelling along the western boundary is associated with the other southward jet. The upwelling on the eastern boundary yields a cool anomaly. Based on field (Klevtsova, 1966; Kosarev, 1970) and satellite observations (Ibraev et al., 1998), such surface current structures and cool anomalies occur in the coastal zone.

Problems due to oil pollution in the Caspian Sea have existed for many years, but they have become particularly urgent recently due to the discovery and development of new, rich deposits of oil on the continental shelf. As long as crude oil is transported across the Sea by ships or pipelines, there will be a risk of spillage and the potential to cause significant pollution of the marine environment. Since it is impossible to totally prevent such accidental spills, nearly foolproof methods should be elaborated for the prediction of the transport and fate of oil spills so that rapid-decision methods can be implemented based on the feasibility and effectiveness of different countermeasures to prevent large-scale disasters.

Once the oil is discharged onto the sea surface, many factors affect it, most of which (including evaporation, emulsification, dissolution, photolysis, and biodegradation) are controlled by properties of the oil. Different oil spill fate processes dominate at different times after the spill and lead to a loss of oil mass (Spaulding, 1988, 1995). For example, evaporation, dispersion, and emulsification are important initially, while biodegradation, photolysis, sinking, and tar-ball formation become important later. In addition, the relative effect of photolysis and biodegradation in the mass balance is small in comparison with the evaporation, dispersion, and emulsification processes.

Surface winds and currents are the most important factors determining the direction and rate at which the oil slick moves. The physical, chemical, and biological reactions which weather or modify oil as it drifts and spreads occur over various time scales ranging from a few hours to months and even years. Thus, to adequately calculate oil fate processes and the transport of oil pollution in the sea, besides the oil's properties, it is necessary to know also the environmental condi-

tions; e.g., winds, currents, waves, turbulence, salinity, temperature, and solar insolation. The main ideas of oil spill and fate modelling have been summarized in reviews by Mackay and McAuliffe (1988) and Spaulding (1988, 1995). An overview of the different modern approaches applied in numerical models of the behaviour and fate of oil spilled in the marine environment presented by Reed *et al.* (1999).

This paper is structured as follows: In the second section, the most important processes affecting oil spill spreading and fate in the marine environment are briefly highlighted; some developments in modelling these processes are discussed as well. In the third section, the structure of the model proposed for modelling oil spills in coastal waters of the Sea is described. In the fourth section, results of modelling oil transport in the Caspian Sea for cases of blowouts in the southwestern part of the Sea are summarized and discussed. In the fifth section, conclusions and recommendations for further improvement of the model are given.

Oil Spill Processes

Techniques exist for the analysis of oil spills, including the presence of various types of oil components in water, sediments, and biota. Modelling of the transport of oil pollution in the ocean takes into account both the mechanical spreading and drift of oil spills and the biochemical processes determining the behaviour of oil and its components in sea water. The use of particle tracking techniques is an example of an effective approach developed recently to numerically simulated oil slicks. This technique is based on the Monte Carlo method. The general approach of this method and its combination with flow models to solve problems of pollution transport have been given (cf. Korotenko, 1994a). In this method, each particle or group of particles represents a fraction of the total oil spill, and their three-dimensional movements are simulated taking into account the effects of the above mentioned physicochemical processes on the fate of the particles (Spaulding, 1988; Proctor et al., 1994; Varlamov et al., 1998; Korotenko & Mamedov, 2000, 2001). To understand these effects, the main mechanisms affecting the oil are described below.

Spreading. Spreading of oil on water is controlled by the driving forces of gravity and surface tension and retarding effects of inertia and viscosity, which lead to an extension of the spilled oil and the formation of a slick on the sea surface. Gravitational spreading generally plays a dominant role within a short period of the order of several hours after an oil spill, while this process of slick deformation may occur over a several-day period (Mackay et al., 1979).



According to the widely used 'thick-thin slick' approach (Mackay *et al.*, 1979), the process of spreading may be arbitrarily expressed as a power function of slick area and thickness:

For a thin slick,

$$\frac{\mathrm{d}A_{\rm t}}{\mathrm{d}t} = C_1 A_{\rm t}^{0.33} \left[\frac{-C_3}{h_{\rm k} + 0.00001} \right];\tag{1}$$

for a thick slick,

$$\frac{\mathrm{d}A_{k}}{\mathrm{d}t} = C_{2}A_{k}^{0.33}(h_{k})^{1.33},\tag{2}$$

where A_t and A_k are total thin and thick slick areas (m²); h_k is slick thickness (m); t is time (s); and C_1 , C_2 and C_3 are constants. These formulas are attractively simple and may yield realistic characteristics of the spreading process but lack a physical basis.

In another approach (Elliott, 1986; Johansen, 1987; Spaulding, 1988) to describing the process of oil slick spreading, oil is modelled as a distribution of droplets that are driven into the sea by breaking surface waves, such that oil spreading is controlled by the droplet size distribution (the droplets have their own buoyancy) and shear diffusion processes.

Advection. Advection is accounted for by simulation of the movement of the centroid of the oil slick due to large scale circulation, tidal, and buoyancy driven and wind-induced transient currents. In the general case, the advection due to the combined effect of these components is described by their vector sum

$$V_{i} = V_{i}^{\text{wid}} + V_{i}^{\text{wad}} + V_{i}^{\text{d}} + V_{i}^{\text{c}} + V_{i}^{\text{T}} + V_{i}^{\text{B}},$$
(3)

where $V_i^{\rm wid}$ and $V_i^{\rm wad}$ corresponds to velocity due to wind drift and wave (Stokes) drift component, respectively which, generally, do not coincide in direction; $V_i^{\rm d}$ is the wind-induced component; $V_i^{\rm T}$ is the tidal component; $V_i^{\rm B}$ is the buoyancy-driven component, and $V_i^{\rm c}$ denotes the large scale component. The sum of the wind induced and Stokes drift components, $V_i^{\rm wid} + V_i^{\rm wad}$, is expressed in terms of wind speed U_A at 10 m above the water surface as $V_i^{\rm wid} + V_i^{\rm wad} = 0.03~U_A$ (Elliott, 1986; Reed et~al., 1989).

Vertical dispersion. Vertical dispersion results from wind-generated breaking waves dispersing oil vertically in the water column. In high sea states where a slick is subject to continual turbulence by wind shear and breaking waves, the oil may be rapidly dispersed into small, i.e., 0.01 to 1 mm diameter drops, which are in the subsurface layer. The simplest approaches employed for description of this process are based on tabulations of dispersion as a function of sea state and time after oil release (Audunson, 1979; Spaulding

et al., 1988). The natural oil dispersion process is very complicated and the exact nature of the fluid mechanics involved is not well understood. The most common supposition is that breaking waves or turbulence cause the oil layer to be propelled into the water column thus forming a "shower" of oil droplets. Most of the oil particles rise again to the slick and coalesce there, but some of the smaller droplets diffuse downward and become permanently incorporated into the water layer, which makes the process of oil transport in the sea essentially three-dimensional. For example, according to in situ measurements (Cretney et al., 1981; Sorstrom, 1987; Genders, 1988), oil has been detected at 20 m depth.

It is likely that the dispersion rate is a function of the slick thickness, oil-water interfacial tension, sea state, and, in particular, the fraction of the sea which is covered by breaking waves (Aravamudan et al., 1982). Based on a series of laboratory investigations on the natural dispersion of oil on the surface and in the water column (Delvigne & Sweeney, 1988), a surface oil slick breaks up into droplets and penetrates into the water due to the turbulence generated by breaking waves. Submerged oil parcels break up into droplets due to turbulence in the ambient water. Hence, the dispersion process due to the turbulence might be treated as the result of a continuous surface source supplying oil droplets with different sizes. A relationship between droplet size distribution, $N_{\rm d}(d)$, and size of a droplet, d, $N_d(d) \approx d^{-2.30(\pm 0.06)}$, where $N_{\rm d}(d)$ is the number of droplets in a unit size interval $[d_0 \pm 1/2\Delta d]$. This relationship holds for all experiments, independent of oil type, weathering state, oil layer thickness, and oil temperature.

The oil entrainment rate Q_R (kg/m² s) per unit area is defined as the dispersed mass of oil in the water column per unit surface area per breaking event. According to the above experiments, Q_R can be expressed as

$$Q_{\rm R}(d) = C(0)D_{BA}^{0.57}S_{\rm COV}F_{\rm WC}d^{0.7}\Delta d, \tag{4a}$$

where $F_{\rm WC} = c_b(U_A - U_{\rm Wi}) T_{\rm W}$ is the fraction of the sea surface covered by overturning waves ('white caps'), $T_{\rm W}$ is the wave period, $U_{\rm Wi}$ is the "initiation of breaking" wind speed (≈ 5 m/s), c_b is constant (≈ 0.032 s/m), $S_{\rm COV}$ is the fraction the sea surface covered by oil, $D_{BA} = 0.0034 \rho_{\rm W} g H_{\rm rms}^2$ is the average energy dissipation per unit surface area in a overturning wave, $H_{\rm rms}$ is the r.m.s. value of the wave height, g is the acceleration due to gravity, C(0) is a proportionality constant dependent on the oil viscosity, μ , at temperature $T_{\rm oil}(K)$: $C(0) \approx [\mu(T_{\rm oil})]^{-1}$, and $\rho_{\rm W}$ is the density of water

In practice, it is convenient to transform Eq. (4a) into a similar equation valid for all different dispersion

sources in terms of dispersed mass per unit surface area per dispersion distortion event. The dispersed mass of oil droplets per unit surface rate and per dispersion event (kg/m²), M(d), is given by $M(d) = C(0)D_{BA}^{0.57}S_{\text{COV}}d^{0.7}\Delta d$ (Delvigne, 1993), from which it follows that the total mass, $M_{\text{tot}}(d_e)$, of dispersed droplets smaller than d_{max} and consisting of the original surface oil is given by

$$M_{\text{tot}}(d_e) = \int_0^{d_{\text{max}}} C(0) D_{BA}^{0.57} S_{\text{COV}} d^{0.7} \, \delta d$$
$$= C(0) D_{BA}^{0.57} S_{\text{COV}} d_{\text{max}}^{1.7}. \tag{4b}$$

The above experiments with different types of oil have shown that maximum droplet size $d_{\rm max}$ depends on turbulence energy level, $E(d_{\rm max} \propto E^{-0.50(\pm 0.1)})$ and oil viscosity $(d_{\rm max} \propto \mu^{-0.34(\pm 0.05)})$. The range of droplet sizes in the experiments was found to be from 5 to 1130 µm, while most of the droplets were concentrated in the range between 75 and 320 µm with a slight tendency for shifting the median of droplet size distribution to small sizes with turbulence duration.

Horizontal dispersion. Another approach is associated with so-called 'slicklets', which are assumed to occur as a result of overturning surface waves forming small patches (slicklets) whose size is presumed to be proportional to the mean wavelength (Aravamudan et al., 1981). The horizontal dispersion of the slicklets is due to the mesoscale surface turbulence.

Turbulent diffusion. When an oil slick is dispersed, an expanding cloud of oil droplets is formed and diffused horizontally and vertically due to turbulence. Some large droplets may rise and reform the slick, but, if the dispersion process is effective, most of them will become mixed into the subsurface layer. A simplified equation for vertical distribution of the oil concentration may be expressed as a function of time and depth:

$$C = C_{\rm S} \exp\left(-z\sqrt{\frac{\pi}{4D_{\rm V}t}}\right),\tag{5}$$

where C_S is the surface oil concentration, z is depth (m), and D_V is the effective vertical diffusivity (m²/s). From examination of experimental data a typical value of D_V is 0.0126 m²/s (Mackay *et al.*, 1979).

For the horizontal diffusion of oil, a simplified equation (Reed, 1989) for the concentration of oil, *C*, can be used

$$C(x, y, t) = (C_0)[erf((D/2 - x)/E) + ((D/2 + x)/E) \times ((D/2 - y)/E) + ((D/2 + y)/E)],$$
(6)

where C_0 is the initial concentration (ppb), erf is the error function, D is the initial cloud diameter (m), and $E = (4K_{xy}t)^{1/2}$. The horizontal diffusivity, K_{xy} (cm/s²),

is calculated according to the Richardson–Obukhov law: $K_{xy} = c_{\epsilon}L^{4/3}$, where c_{ϵ} is an empirical constant chosen to be dependent on the turbulence dissipation rate (\sim 0.01), and L (cm) is the scale of the phenomenon (cf. Ozmidov & Korotenko, 1989).

These simplified equations for vertical and horizontal turbulent diffusion processes provide a very coarse description. More accurate calculations of diffusive oil transport require use of numerical models of turbulence and turbulent transport (Korotenko & Mamedov, 2001).

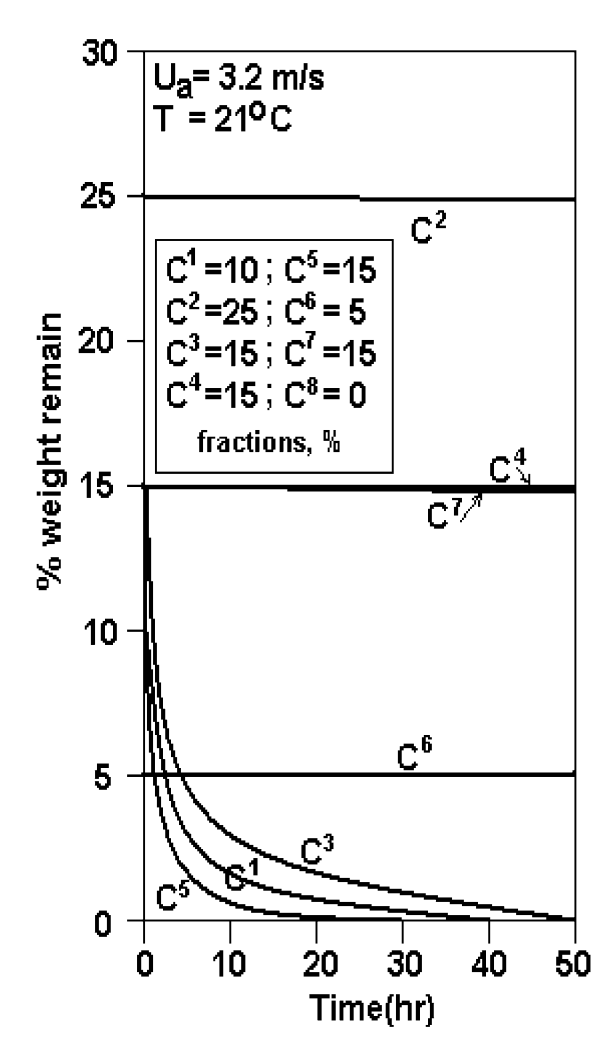
Evaporation. Evaporation is a very significant mass loss for many kinds of oil and it has a profound effect on density and viscosity and other properties of oil. Evaporation can account for the loss of up to 60% of spilled light crude oil. Rates of the evaporation depend on the oil vapour pressure, as influenced by composition and temperature, and on transport characteristics of the air–sea boundary layer influenced primarily by the wind. The vapour pressure changes as hydrocarbon fractions are lost into atmosphere. Among methods developed for modelling evaporation, an analytical approach and pseudo-component approach are widely used. The analytical approach develops an expression for the vapour pressure as a function of the degree of evaporation or weathering (Mackay et al., 1983).

In the pseudo-component approach, oil is characterized by a set of hydrocarbon components grouped by molecular weight (Spaulding *et al.*, 1988) or by boiling point fraction (Payne *et al.*, 1984). This approach allows different fractions of the oil to evaporate at different rates depending on the fraction considered. Owing to the large number of individual components in crude oils, Moore *et al.* (1973) suggested simulating them by incorporating eight components (see also Yang & Wang, 1977; Proctor *et al.*, 1994; Sebastiao & Guedes Soares, 1998) or 27 single pseudo components (Reijnhard & Rose, 1982).

The range of physical and chemical properties of eight individual hydrocarbon fractions is usually considered in models are presented in Fig. 3, left. These groups are: the lower alkanes (which are quite volatile, have solubilities in excess of 10 mg/1, and generally lie in the C^3 to C^7 range including cycloalkanes); the higher alkanes (which are less volatile and soluble and have eight or more carbons); the mono-aromatics (benzene); the naphthalenes; the higher poly-cyclic aromatics; and an inert residue. An example of weight changes of individual fractions of light crude oil (no. 2 according to the classification given by Yang & Wang, 1977) with constant wind speed and air temperature is also considered (Fig. 3, right).

The mass transfer rate, dm_i/dt , due to evaporation is given by Reed *et al.* (1989)

Description	Density (q/ml)	Boiling Point (C)	Molecular Weiaht
Paraffin C6-C12	0.66- 0.77	69-230	86-170
Paraffin C ₁₃ -C ₂₅	0.77- 0.78	230- 405	184-352
Cydoparaffin C6-C12	0.75-0.9	70-230	84-164
Cydoparaffin C13-C23	0.9-1.0	230- 405	156-318
Aromatic (mono- and di-cydic) C6-C11	0.88-1.1	80-240	78-143
Aromatic (poly- cyclic) C12-C18	1.1-1.2	240- 400	128-234
Naphtheno- Aromatic C9-C25	0.97-1.2	180- 400	116-300
Residual (induding heterocydes)	1-1.1	400	300-900



Typical Hydrocarbon Component of Oil Spill.

Oil Spill Component versus Time (Changes due to evaporation).

Fig. 3 Range of constants for hydrocarbon fractions (left) and the per cent weight changes of individual fraction of a light crude oil versus time (right) (modified from Yang & Wang, 1977).

$$\frac{\mathrm{d}m_i}{\mathrm{d}t} = \frac{K_{\mathrm{E}}M_i P_i}{RT_{\mathrm{oil}}} A_{\mathrm{S}} f_i,\tag{7}$$

where M_i is molecular weight (g mol), P_i is vapour pressure (atm), A_S is spilled area (m²), and R is the gas constant. Following Mackay and Matsugu (1973), the mass transfer coefficient for evaporation K_E is calculated as

$$K_{\rm E} = 0.028 U_A^{0.78} D_{\rm S}^{-0.11} S c_i^{-0.67},$$
 (8)

where D_S is the spillet diameter (m) and Sc_i is the Schmidt number of the *i*th fraction.

The evaporation process results in an increase of oil viscosity, μ . This increase can be expressed as (Mackay *et al.*, 1979)

$$\mu = \mu_0(C_\mu F_{\rm E}),\tag{9}$$

where $F_{\rm E}$ is a fraction evaporated, μ_0 is the parent oil viscosity, and C_{μ} is of the order 1–10 and chosen to be dependent on oil type.

Emulsification. Many oils tend to absorb water to form emulsions which may contain up to 80% water. Thus, emulsification is an important process for certain oils which apparently have chemical constituents which favour the formation and stability of emulsified water. Stable emulsions may contain 80% water, are very viscous, and have densities approaching that of sea water. Water-in-oil emulsions are often light brown in colour and are referred as 'chocolate mousse'. The rate of emulsification increases with increasing sea state and can be described by the formula (Mackay et al., 1979)

$$\frac{dY_{W}}{dt} = K_{A}(1 + U_{A})^{2}(1 - K_{B}Y_{W}), \tag{10}$$

where Y_W is fractional water content, $1/K_A$ is the final fractional water content (0.8), K_B is an empirical coefficient (\approx 1.43), which is chosen to be dependent on wind speed, U_A . The water is present in the emulsion in the form of small droplets. Since oil is unable to shear through such droplets and has to flow around them, there is an increase in the force necessary to generate a given shear rate or velocity gradient. This effect is (by definition) an increased viscosity. Such an increased viscosity may exceed the viscosity of the incorporated parent oil by several orders of magnitude. Thus, the emulsification process is also accompanied by an increase in the effective oil viscosity (Mackay *et al.*, 1979)

$$\mu = \mu_0 \exp\left(\frac{2.5Y_{\rm W}}{1.0 - 0.65Y_{\rm W}}\right). \tag{11}$$

Density increase. The processes of evaporation and formation of water-in-oil emulsion lead also to an increase in the oil density. Due to weathering, the density of few crude oils may exceed the water density. However, the density of many water-in-oil emulsions approaches that of water and, therefore, requires very little uptake of particulate matter to cause the emulsions to submerge. Temperature changes may also cause floating oils to sink and then resurface later. The algorithm used to calculate oil emulsion density $\rho_{\rm E}$ (kg/m³) is (Buchanan and Hurford, 1988)

$$\rho_{\rm E} = Y_{\rm W} \rho_{\rm W} + (1 - Y_{\rm W})(\rho_{\rm c} + C_{\rho} F_{\rm E}), \tag{12}$$

where $\rho_{\rm c}$ is the density of the original crude oil and C_{ρ} is constant obtained from distillation data.

Dissolution of hydrocarbons from a slick is generally unimportant for the spill mass balance because less than 1% of the oil slick may dissolve. Such a low dissolution of oil is a result of three factors: (1) the low dissolution mass transfer coefficient; (2) the very small water solubility driving force; and (3) the presence of relatively small quantities of the more soluble hydrocarbons, most of which are more susceptible to evaporation. The dissolved concentrations in water under an oil slick have been of concern from a toxicological viewpoint. Measured concentrations, however, have been less than 0.1 mg/l (McAuliffe, 1986).

Photolysis is also an important process for slick weathering from the formation of oxygenated species, resulting in changes in interfacial properties (affecting spreading and water-in-oil mousse formation) and possibly leading to the transfer of relatively toxic organic species to deep layers. Much of the toxic burden in the water column, for example, is attributable to

these photolytic products, as distinct from hydrocarbons present in the oil. This process, however, is unimportant over the first few days of a spill but may become significant after a week or more (Spaulding, 1988).

Modelling of the photolysis of an oil slick has suffered from the lack of knowledge of the mechanisms, reaction rates, and photolytic products which vary with oil composition and level of the insolation. In oil spill model of Cochran and Scott (1971), a formulation for the rate of photo-oxidation is proposed as

$$\frac{\partial P}{\partial t} = \left(\frac{B}{70}\right)(1 - C)C_A,\tag{13}$$

where B is the sun's radiating angle (°) to the slick surface, C is the fractional cloud cover, and C_A is a coefficient that varies with the slick thickness.

Sinking/sedimentation of oil may occur when, as a result of evaporation and emulsification processes (see above), its specific gravity is greater than that of the water, although it is a minor factor causing the oil to submerge. It is more likely that the presence of sediments will cause a significant portion of the spilled oil to flocculate and then sink to the bottom. A number of laboratory studies have indicated that size, type, and load of sediments; the salinity and some properties of the oil; such as, its of sulphur and organic matter contents; and degree of agitation affect the adsorption/desorption of oil onto sediment particles. Based on experimental results (Kolpack *et al.*, 1977), the rate of oil loss due to the oil-sediment adherence process, dA_d/dt (m³/s), is given as

$$\frac{\mathrm{d}A_d}{\mathrm{d}t} = 1.4 \times 10^{-12} S_{\mathrm{L}} (1 - 0.023 S_a),\tag{14}$$

where S_L is sediment load (gm/m³) and S_a is salinity.

Biodegradation is an extremely slow process which only becomes important in the long-term in the removal of oils from the marine environment. Degradation rates are difficult to predict because of high hydrocarbon dilution, variations inherent in hydrocarbon degradability (such as types and numbers of microbes), and nutrient and oxygen status of dilution waters. Because of the complexity of the process, most of the studies of microbe-hydrocarbon interaction have been carried out under controlled laboratory conditions, and their results are assumed applicable to the aqueous environment. Presently, calculations of the mass loss of oils in long-term models are based on databases which contain the halflife of hydrocarbons in the marine environment (Feng et al., 1989).



Oil Spill Model

The description of the transport and dispersion of a contaminant spilled at sea may be based on the advection-diffusion equation solved by finite differences for the concentration, C

$$\frac{\partial C}{\partial t} + U_i \frac{\partial C}{\partial x_i} = \frac{\partial}{\partial x_i} \left(K_{ij} \frac{\partial}{\partial x_i} \right) + S, \tag{15}$$

where U_i are the components of the three-dimensional mean velocity field, K_{ij} is the diffusion tensor, and S is a source or sink term.

Instead, to simulate oil spill spreading, it is suggested that the model use the pre-calculated mean velocity and the random walk (Monte Carlo) technique to follow the motion of individual particles (oil droplets), the total amount of which constitutes the oil spill. As has been shown by Hunter (1987), models based on the random walk concept are significantly more effective than the finite-difference method mainly because the former exactly describes the advection, which is the most important transport process for oil slicks.

Transport model description

The basic concept of this approach (Fig. 4) is similar to that of Proctor *et al.* (1994), except that oil is initially divided into fractions in order to describe the evaporation process with more accuracy.

The main part of the model is Block 5 where displacements of each particle are estimated as given by the following expressions (Korotenko, 1992, 1994b):

$$(\Delta x_i)_{j,k} = V_{i,j} \Delta t_j + (\eta_i)_{j,k} \quad (i = 1 - 3; \ j = 1, 2 \dots, N_t; k_f = 1, 2, \dots, N_f; \ f = 1, 2, \dots, 8)$$
(16)

The displacements, $(\Delta x_i)_{j,k}$, are defined as the deterministic part of the motion due to the mean velocity field, $V_{i,j}$, and the random displacement, $(\eta_i)_{j,k}$, due to fluctuations of velocity and denotes the displacement of the kth particle moving along the x_i -axis at the jth instant of time, N_t is the number of time steps, Δt is the time step, N_f is the number of particles in each fraction, and the subscript f denotes a particle fraction.

The distribution of the number of particles in fractions (hydrocarbon groups) is initially assigned and distributed randomly depending on the type of oil. The total number of the particles launched in the model usually does not exceed 106; nevertheless, the behaviour of the tracked particles proved to be representative of the entire spill, even though each droplet represents only a small part of the total volume of the oil. Within each fraction, each droplet is also randomly distributed to have its own half-life according to the empirical exponential laws (Fig. 3, right). In practice, those distributions are assigned randomly by means of a random number generator giving uniform numbers chosen uniformly between 0 and 1, and then they are transformed into an exponential distribution with a weight dependent on wind speed and oil temperature (Eqs. (7) and (8)). The 'long-living' fractions such as C^2 , C^4 , C^6 , C^7 , and C^8 are randomly exponentially distributed within a range corresponding to the rather slow effect of total degradation. Their halflife for total degradation is chosen to be 250 h (Proctor et al., 1994).

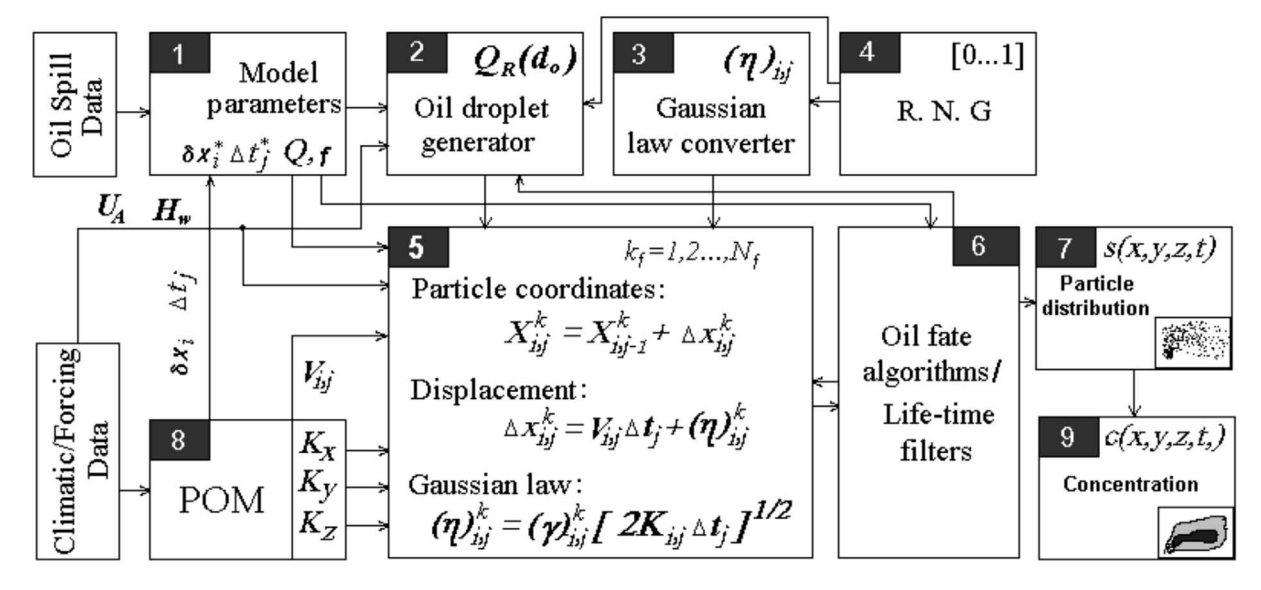


Fig. 4 Schematic of principal elements of the hybrid model.

In addition to the regular movements due to mean current velocity, oil droplets experience a random diffusion due to velocity fluctuations, the distribution law of which is represented by the term, $(\eta_i)_{i,k}$, the latter being, in the general case, a function of time and space. The type of law for $(\eta_i)_{i,k}$ is determined by the statistical structure of deviations (fluctuations) of velocity from its mean value at each time step Δt . Since these fluctuations are considered independent, the law for $(\eta_i)_{ik}$ is thought to be Gaussian (Monin & Yaglom, 1965). In this case, the $(\eta_i)_{j,k}$ can be represented as $(\eta_i)_{j,k} = \gamma_{j,k} (2K_{i,j}\Delta t)^{1/2}$, where $\gamma_{j,k}$ is a random vector normally distributed with an averaged value of zero and unit standard deviation; $K_{i,j}$ represents coefficients of diffusion along the x_i -axis at the time $t_i = t_0 + j\Delta t$. The random vector, $\gamma_{i,k}$, is obtained with the use of the random number generator, Block 4, giving a homogeneous distribution of random numbers between 0 and 1, with consequent transformation to the Gaussian law in Block 3. The horizontal and vertical diffusion coefficients, $K_{x,j}$, $K_{y,j}$ and $K_{z,j}$, as well as the mean current velocity U_i^j are provided by the flow model (Princeton ocean model, POM), Block 8. In the 'oil spill data' block, the location and configuration of source(s), its (their) regime of release and production rate, and type of oil and hydrocarbon groups are collected for subsequent initialization in Block 1, where initial parameters such as the size of the investigated area, spatial resolution and time steps are adjusted to those used in the flow model, Block 8.

In Block 3, the particles diameters, d_0 are assigned randomly in the range d_{max} – d_{min} . The entrainment rate, $Q_{\rm R}(d_0)$ is defined as a function of U_A and $H_{\rm rms}$ (Eq. (4a)). The critical diameter, d_c , (Aravamudan et al., 1982) is given by the expression $d_c = (9.52v^{2/3}/$ $g^{2/3}(1-\rho_0/\rho)^{1/3}$). The buoyancy force depends on the density and size of the droplets and the vertical velocity, w, (Proctor et al., 1994) which can be estimated as $w = (gd^2(1 - \rho_0/\rho)/18\nu)$ for small droplets $d \le d_c$, and as $w = \left[(8/3)gd(1 - \rho_0/\rho) \right]^{1/2}$ for large droplets $d > d_{\rm c}$. Hence, the larger droplet sizes are more buoyant and tend to remain near the sea surface, while the smaller droplets are less buoyant and could be transported downwards due to turbulence. Each particle, droplet or slicklet k belonging to fraction f is characterized by its size, density, position $X_{i,i}^k$, age and its own 'half-life', the latter being assigned a priori when the particle is launched.

The transport model includes the effects of evaporation, emulsification, and decomposition, the latter due to biochemical and physical degradation. Algorithms for these effects are incorporated in Block 6, and they are parameterized in terms of 'half-life' time filters which compare current time and the 'half-life' time assigned for each particle. Only particles that occur within the subsurface 'evaporation layer' of

thickness, z_{ev} (0.1 m), experience evaporative decay, while particles at all depths in the water column experience disintegration.

The model takes into account the beaching of oil: If the oil droplet reaches the coastline, it is marked as beached. In the former case, the droplet is fixed at the point where it reached the beach, while, in the latter case, the droplet is reflected back to sea and remains in the computational process.

Finally, data of coordinates $S_j = \{(X_1; X_2; X_3)_j\}$ are stored in Block 7, the latter being also used for identification of space cells where each particle is found at time t_j . The particle concentration C(x, y, z, t) in a cell is defined in Block 9 as the number of particles found in the cell relative to the volume of the latter. In this block, the particles remaining in the water column, at the sea surface, beached, and decayed are counted separately and inventoried in an updated summary.

Flow module

The complex dynamics and thermodynamic of coastal waters, synoptic atmospheric forcing, and influences of river discharge and evaporation require application of a high-resolution circulation model in both the horizontal and vertical directions, approximately 1/12 min and 1 m (for upper layer of the sea), respectively, for the model to produce adequate simulations. From Block 8, the sigma-coordinate (terrain following) primitive equation POM (Blumberg & Mellor, 1987) was implemented for the simulation of large scale, V_i^c , and wind-driven, V_i^d , currents. To compute the former, the model was forced by pseudomonthly averaged wind stress, and, to compute the latter, it was forced by synoptic winds for the winter and summer seasons. The surface stress was calculated with a drag coefficient, C_A , chosen to be either dependent on wind speed, U_A , i.e., $C_A = 1.10 \times 10^{-3}$ for $U_A \leq 6$ m/s and $C_A = 0.61 \times 10^{-3}$ for $U_A > 6$ m/s. The bottom stress was calculated with a drag coefficient chosen to be either dependent on grid size or a constant, 0.0025 in case of a grid with low resolution (Blumberg & Mellor, 1987). The tidal currents in the Caspian Sea are negligible, so $V_i^{\rm T}$ was set to zero.

The horizontal diffusion coefficients, $K_{x,j}$ and $K_{y,j}$, were calculated in POM from Smagorinsky formula, while the vertical diffusivity, $K_{z,j}$, was obtained from the level 2.5 turbulence model (Mellor & Yamada, 1982).

Implementation for the Caspian Sea

The model grid area covers the entire Caspian Sea from 38°40′ to 47° N and from 47° to 54° E. The grid size is 1/6 degree in the both zonal and meridional



directions. The model grid has 21 sigma levels non-uniformly distributed with high resolution near surface and near bottom. It was initialized with seasonally averaged climatic temperature, salinity fields. Initial climatic velocity was chosen according to the "classical" scheme (Fig. 1, right). These seasonal characteristics were used as the initial background condition for calculation of short-term variations due to synoptic winds. The probability of occurrence of various wind directions in summer and winter (Tables 1 and 2), was used for simulations of drift currents and oil spreading. Southeastward and southwestward winds are the most prevalent winds for both seasons. Based on surface drift currents generated by steady southeastward and southwestward winds of 10 m/s the circulation is strongest in the extensive shallow shelf areas, taking the form of coastal jets (Fig. 5). This effect was also noted numerically by Ibraev et al. (1998). The jet-like structure of the surface currents appears along both the western and eastern boundaries, the latter being in contradiction to the general scheme of circulation suggested earlier (Ledney, 1943), as mentioned above. Under non-stationary windforcing, strong changes in the upper layer circulation occur within a few days in numerical simulations, as has also been noted numerically by Badalov & Rzheplinsky (1989).

Before simulating the transport of oil slicks, a number of initial parameters had to be specified. The oil (Gunashly type) was specified by density $\rho_{\rm oil} = 872$ kg/m³, droplet diameters, $d_{\rm min} = 60$ µm and $d_{\rm max} = 600$ µm, the evaporation times, and 'half-life times'

 $T_{\rm ev1}=20$ h, $T_{\rm ev3}=30$ h, $T_{\rm ev5}=10$ h, for the fractions C^5 , C^1 and C^3 , respectively. For the 'long-living' fraction, C^2 , C^4 , C^6 , C^7 , and C^8 , as mentioned above $T_{\rm ev4}=250$ h. A percentage ratio between C-fractions, which a priori was set initially during a distribution of droplets between fractions for the light crude oil was the following: C^1 , C^2 and $C^8=15\%$; C^3 and $C^4=20\%$; $C^5=5\%$; $C^6=3\%$; $C^7=7\%$. These ratios mean that about 40% of oil is predicted to be evaporated within the few first days.

Since the transport model was designed in a z-level coordinate system, the simulated velocity and diffusivity data from POM were converted from sigma levels to z-levels and, linear interpolation between the two types of levels was implemented. The transport model had 400 vertical levels; the vertical resolution, Δz , was 0.1 m. The horizontal resolution, Δx and Δy , of both models was similar. Time steps for the flow model were 6 and 180 s corresponding to the external and internal modes of POM, respectively, and 1800 s in simulations of droplet transport.

A hypothetical 10-day blowout scenario releasing light crude oil was investigated in terms of its potential for delivering oil to the beaches of Azerbaijan and Iran. The release point was chosen to be at 39°25′ N, 50° E, in the coastal waters of Azerbaijan, approximately 140 km south of Baku (Fig. 1), in the region of intensive development of oil deposits. For each time step (1800 s) the hypothetical source emitted 100 droplets, which means that, by the end of the blowout, the total number of released droplets was 48,000. Calculations covered a 30-day period.

Table 1	1 Probability	(%) of	different	wind	directions	in	summer

Wind speed m/s	Wind direction	on						
	N	NE	Е	SE	S	SW	W	NW
0	7.24	0.02	0	0	0	0	0	0
0-5,0	4.28	5.48	3.5	5.44	1.87	1.71	1.75	5.46
5,0-7,5	11.53	8.50	3.45	5.45	2.29	1.48	1.60	11.5
7,5–12,5	4.61	1.81	0.56	1.04	0.31	0.15	0.1	5.7
12,5–17,5	0.81	0.14	0	0.04	0.02	0	0	1.87
17,5–22,5	0.04	0	0	0	0	0	0	0.22

Table 2 Probability (%) of different wind directions in winter

Wind speed m/s	Wind direction									
	N	NE	Е	SE	S	SW	W	NW		
0	6.32	0	0	0	0	0	0	0		
0-5,0	2.98	5.54	3.92	4.9	1.88	1.82	1.26	3.38		
5,0-7,5	7.7	10.18	5.5	7.8	3.7	2.9	1.58	6.98		
7,5–12,5	4.42	2.72	1.27	2.4	1.16	0.8	0.2	4.16		
12,5–17,5	1.12	0.32	0.1	0.36	0.14	0.1	0	1.86		
17,5–22,5	0.12	0.02	0	0.02	0	0	0	0.32		

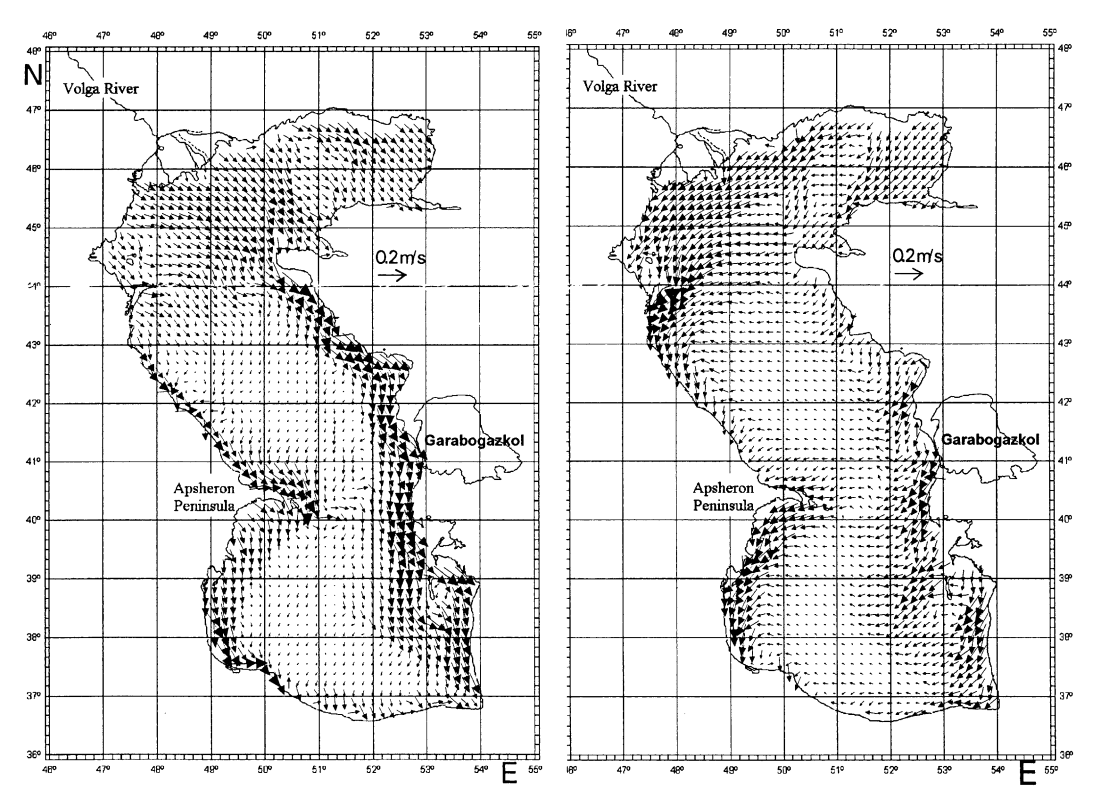


Fig. 5 Wind drift component of the currents under (a) southeastward and (b) southwestward winds.

Results and Discussion

Since sustained steady winds are extremely rare for the Caspian Sea (Ikonnikova, 1960), the numerical experiments were mostly carried out for conditions of varying wind direction with the probability of its direction chosen from Tables 1 and 2. Two types of scenarios for the oil spill experiments were used: with 'regular' winds and with random winds. In the first type of experiment, it was assumed that the wind changed direction regularly while the duration of each wind direction was taken in correspondence with Tables 1 and 2. In the second type of experiment, it was assumed that the wind direction changed randomly, while its direction was also taken from the Tables 1 and 2.

An example of a 'regular wind experiment', the wind was chosen to change its direction clockwise starting with the northwestward, i.e., the sequence of its direction was the following: NW–N–NE–E–SE–S–SW–W. Wind speed was assumed constant and equal to 7.5 m/s. The computations were performed for 30 days; for this period, the wind velocity vector was supposed to make a complete turn of 360°, while the duration of action of the wind in a given direction was chosen to be dependent on the probability of its occurrence (Table 1). The droplet density (concentration), *N*, in the sea surface layer is examined for 5, 10, 15, 20, 25 and 30 days after the release (Fig. 6). For the

first 5 days following the beginning of the oil release, winds were predominantly southeastward. The computed slick was a slightly elongated patch (75×50) km²), and its leading edge crossed 39° N (Fig. 6(a)). Within the next 10 days, the wind direction changed gradually from southeastward to from the southwestward, which resulted in further extension of the whole oil slick moving southward. By the 10th day, the leading edge reached 38° N, and the patch became more elongated (Fig. 6(b)). The further rapid southward translation during the next 5 days resulted in the patch reaching the Iranian coast, and the slick covered a large area (ca. $225 \times 100 \text{ km}^2$, Fig. 6(c)). During this 5-day interval, oil began beaching along the coast of Iran; approximately 2% of all oil had beached by the 15th day after the release. More oil beached during the next 15 days. During this period, the wind direction had changed from westward to northwestward, forcing the leading edge to move along the Iranian coast to the coast of Azerbaijan (Fig. 6(d)–(f)). The calculated oil fate as a history of oil released, oil evaporated and decayed, oil remaining in seawater, and oil beached in this experiment is summarized in Fig. 7.

Another 'regular' numerical experiment is considered for the winter (Fig. 8). Starting with a northward wind, the oil slick began to move rapidly to the Apsheron Peninsula; however, a relatively quick change of wind direction to southward forced the oil slick southeastward to the coasts of Turkmenistan and

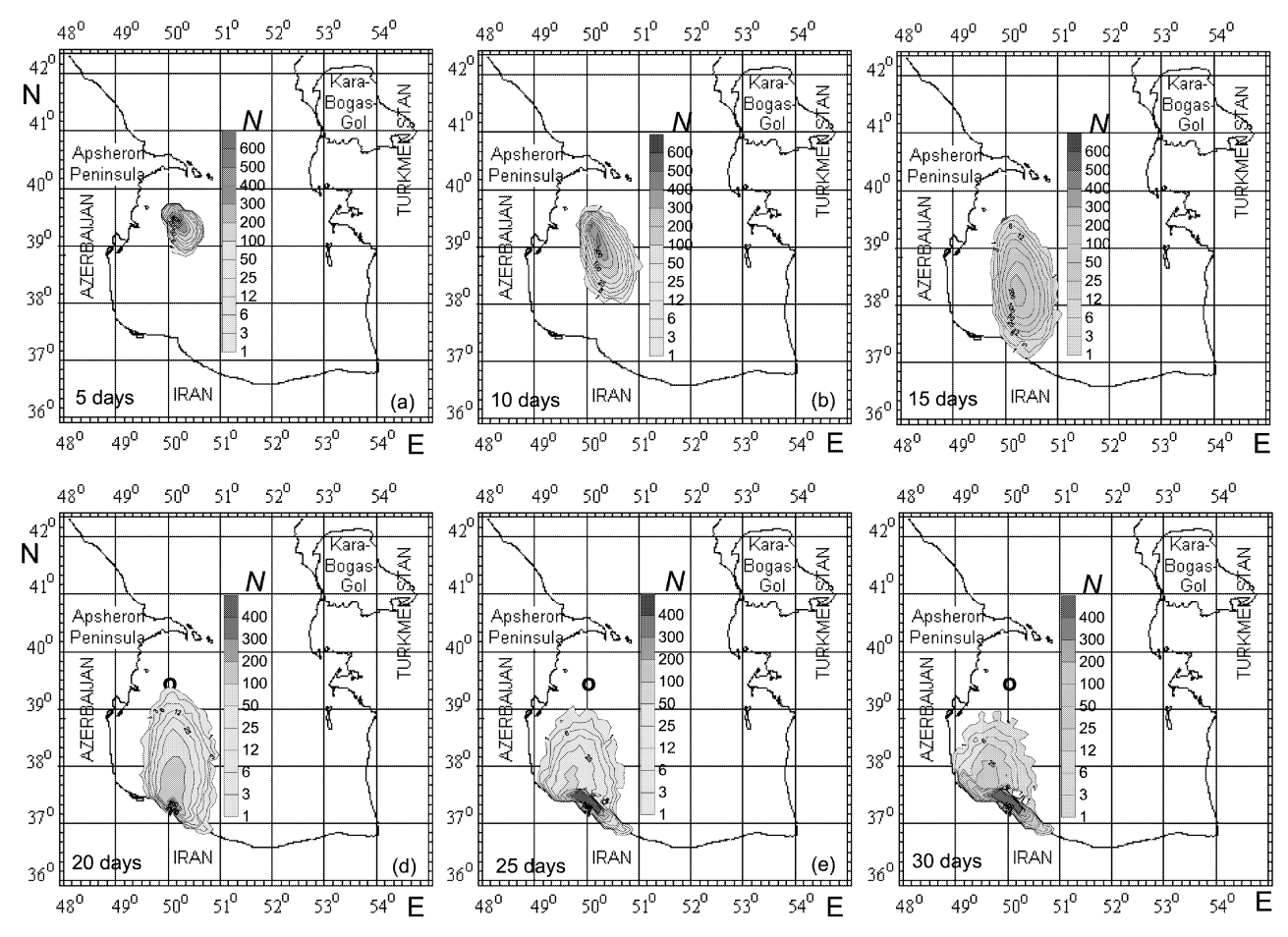


Fig. 6 Successive phases of the oil spill moving under predominant southeastward wind.

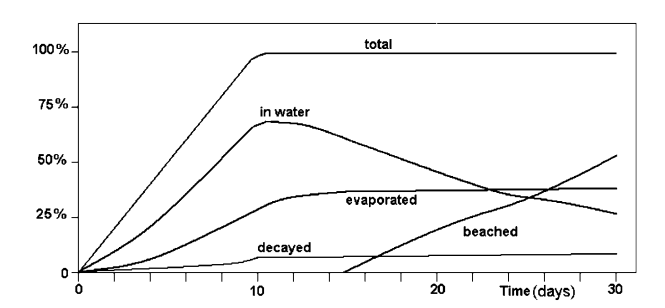


Fig. 7 Time series of modelled oil components for the case presented in Fig. 9.

Iran. By day 30 the oil slick reached Turkmenian coast.

One of the worst scenarios for the Azerbaijan coast occurs when oil is released with initial westward winds. In such a scenario, the sequence of wind direction was the following: E-SE-S-SW-W-NW-N-NE. The prevalence of westward and northwestward winds at the beginning of the experiment led to a rapid approach of the oil slick to the Azerbaijan coast (Fig. 9). It took about 3 days to reach the shoreline. The

change of wind direction according to this scenario led to extremely extensive polluting of the Azerbaijan coast.

Numerical experiments were performed with steady winds which could present a serious hazard to the beaches of Azerbaijan and Iran with the aim of assessing the probability of delivering oil to the coasts. Predicted oil mass was estimated from the percentage of oil reaching the shore (Tables 3 and 4). For the Azerbaijan coast, the beached amount was predicted to be in the range of 15–25% of the total amount released. Southward and southwestward are predicted to be the most hazardous wind directions for the Iranian coast. In this case, the minimal time taken for the oil slick to beach oil is predicted to be about 4 days. The relatively short time necessary for an oil spill to reach the coast in these experiments implies that the major mass loss is due to evaporation, while the other destructive processes make minor contributions.

As is seen from Tables 3 and 4, for similar wind conditions the estimated time for beaching is different for the winter and summer, i.e., the time necessary for slicks to reach the shore was found to be shorter for a

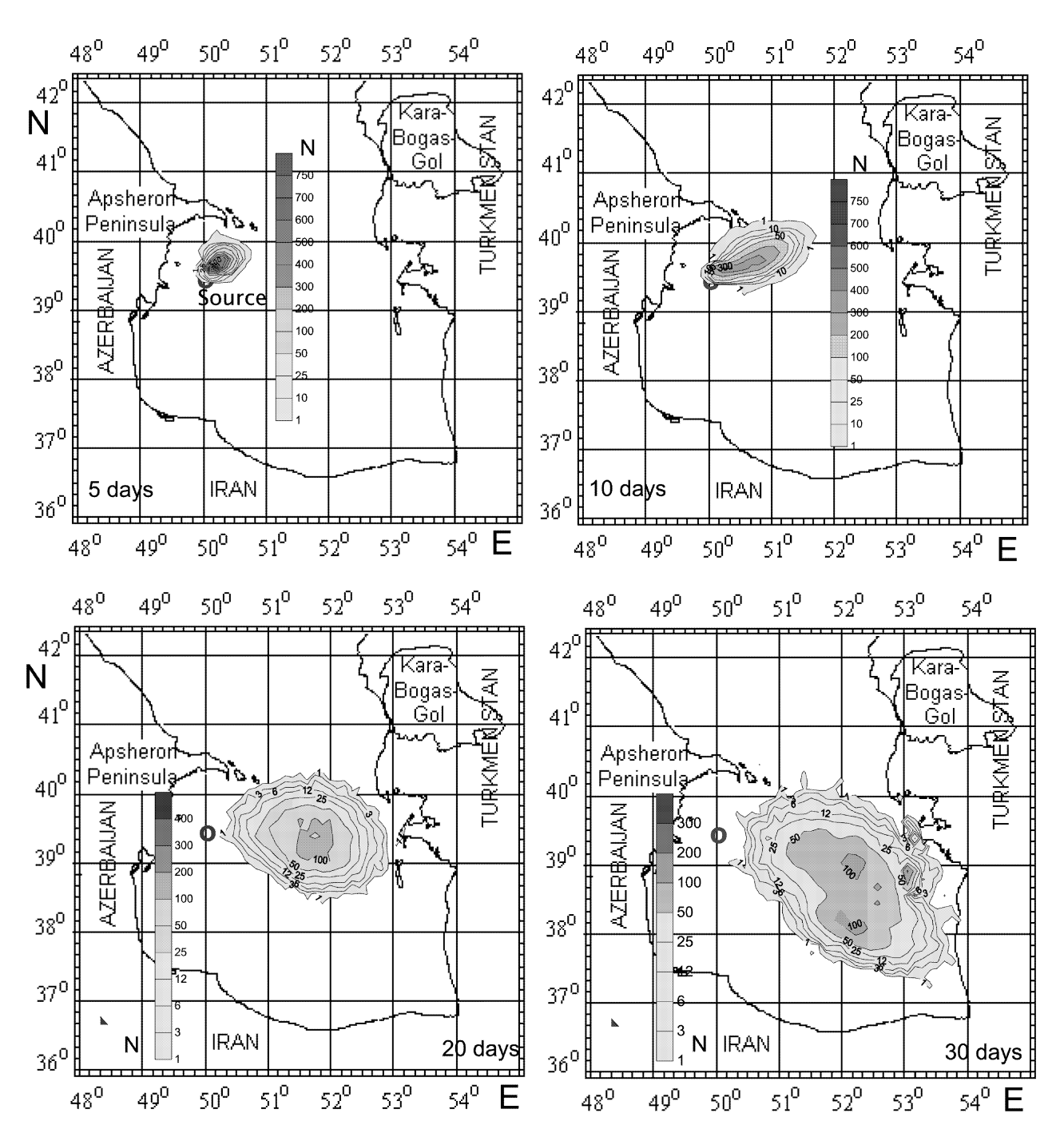


Fig. 8 Successive phases of the oil spill moving under predominant northward wind.

typical summer period. The explanation for this effect seems to be the 'diurnal jet' (Price et al., 1986) which is formed in a stratified surface layer under intensive solar heating and moderate winds. Such conditions create a thin near surface sublayer which slides over the stratified layer. This effect on matter transport in the surface layer is very important for matter transport and was investigated theoretically and in field and numerical experiments by Ozmidov & Korotenko (1989) and Korotenko (1992). Strong winds (more

than 8 m/s), however, were found to destroy the stratification and the diurnal jet; thus, conditions for transport are likely to be equivalent for both seasons. This effect was found by present numerical experiments carried out with winds of 12.5 m/s (Table 3).

Conclusion and Future Development

As with most of oil spill transport models, the model presented in this paper is divided into three



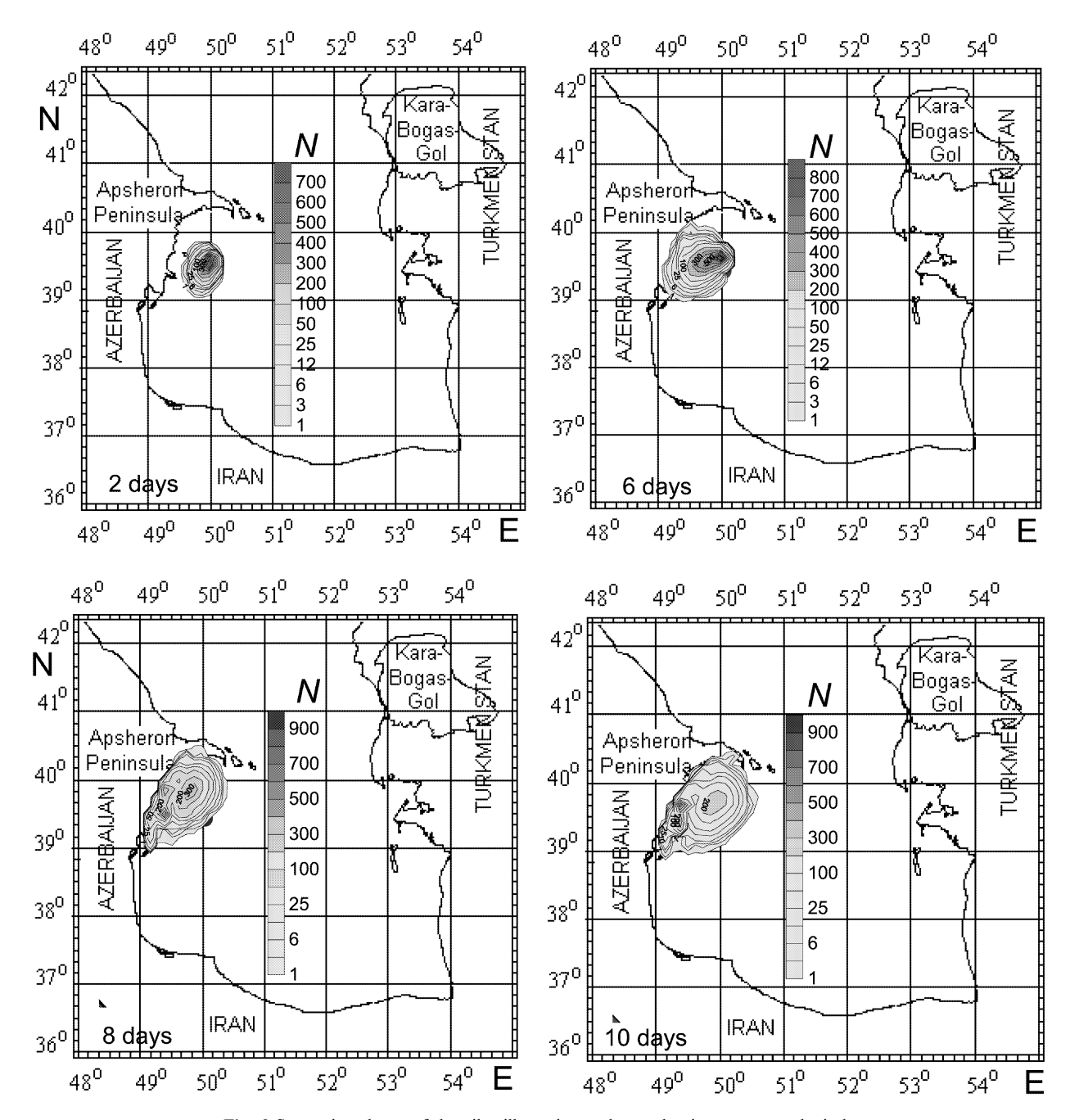


Fig. 9 Successive phases of the oil spill moving under predominant westward wind.

Table 3 Predicted time and fractional of oil transported to the Azerbaijan coast

Season	Wind		Estimated time for	Predicted total amount of beached oil (%)	
	Direction	Speed (m/s)	reaching coast (h)		
Winter	Westward	7.5	56	89	
Summer	Westward	7.5	50	85	
Winter	Northwestward	12.5	56	87	
Summer	Northwestward	12.5	56	83	
Winter	Northward	7.5	93	84	
Summer	Northward	7.5	87	79	



Table	4 Predicted	time and	fractional	of oil	transported	to t	the 1	Iranian c	oast
-------	-------------	----------	------------	--------	-------------	------	-------	-----------	------

Season	Wind		Estimated time for	Predicted total amount
	Direction	Speed (m/s)	reaching coast (h)	of beached oil (%)
Winter	Southward	12.5	130	70
Summer	Southward	12.5	125	61
Winter	Northwesterly	12.5	92	74
Summer	Southeastward	12.5	88	72

major modules: input, trajectory and fate prediction algorithms and output; the latter, in turn, is subdivided into the oil data output and environmental data output. The oil spill prediction procedure is split into two parts: (1) the computation of the current field by means of the POM and input of these currents together with winds to the oil spill transport model; and (2) the oil spill model which uses a random walk particle-tracking method, together with the currents from (1), to predict the three-dimensional movements and fate of oil droplets. Among the processes affecting the fate of oil, advection, turbulent diffusion, evaporation, and decay are included; the decay is modelled as the combined effect of all the biochemical and physical mechanisms that decompose oil.

The combination of incident-specific environmental data and spilled oil characteristics, allows conducting diagnostic and prognostic simulations of behaviour of the oil slick in the marine environment.

The transport model has been implemented for the southern part of the Caspian Sea to predict oil slick movement and the area covered by the oil; also, risks of coastline contamination by the beaching of oil spills in coastal waters were illustrated. Hypothetical 10 day blowout scenarios releasing light crude oil in the southwestern part of the Caspian Sea, where intensive and extensive development of oil deposits is expected soon, have been investigated in terms of the potential for beaching oil under different wind conditions for two seasons. The worst scenarios for the coasts of Azerbaijan and Iran occur with westward and southwestward winds, which have been investigated to estimate the amount of beached oil in each case.

Future improvement of the model is likely to include, on the one hand, high resolution nesting flow submodel and, on the other hand, the model will be incorporated into an integrated environmental monitoring system to provide real-time forecasting (see Elliott and Jones, 2000) instead of hindicasting studies. Besides of POM it is expected that the high resolution, low-dissipative DieCAST (Dietrich, 1997) model to be used in the integrated system.

Since for adequate prediction of vertical transport of oil and other dispersant thermal stratification is very important during the spring and summer periods for Caspian Sea it will need to be thoroughly modelled. Correct description of upper ocean turbulence and process of formation of oil into droplets due to it (Li & Garret, 1998) the subduction of iol droplets to deep layers by action of surface waves (Thorpe, 1995) are objectives for future research.

Acknowledgements—Authors are grateful to Professor A.J. Elliott for fruitful discussion on paper and valuable remarks. The work was carried out in the framework of the Fulbright project no. 23945 and partly under MacArthur grant no. 00-62805.

References

Aravamudan, K.S., Ray, P., Marsh, L.G., 1981. Simplified models to predict the breakup of oil on rough seas. Proceedings of 1981 Oil Spill Conference, American Petroleum Institute, Los Angeles, USA, pp. 153–159.

Aravamudan, K., Ray, P., Ostund, J., Newman, E., Tucker, W., 1982. Break up of oil on rough seas-simplified models and step-by-step calculation. Report no. CG-D28-82, US Coast Guard, NTIS no. ADA118, p. 372.

Audunson, T., 1979. Fate of oil spill on the norwegian continental shelf. Proceedings of 1971 Oil Spill Conference, American Petroleum Institute, Los Angeles, pp. 163–168.

Badalov, A.B., Rzheplinsky, D.G., 1989. Modeling of the Caspian Sea upper layer dynamics under the forcing by synoptic atmospheric processes. In: Sarkisyan, A.S. (Ed.), Modeling of Hydrophysical Processes and Fields in Closed Basins and Seas, Moscow, Nauka, pp. 31–51 (in Russian).

Blumberg, A.F., Mellor, G.L., 1987. A description of a threedimensional coastal ocean circulation model. In: Heaps, N. (Ed.), Three-Dimensional Coastal Ocean Models, vol. 4, AGU, Washington, p. 208.

Bondarenko, A.L., 1993. Currents of the Caspian Sea and formation of salinity of the waters of the north part of the Caspian Sea. Moscow, Nauka, p. 122 (in Russian).

Buchanan, I., Hurford, N., 1988. Methods for prediction of the physical changes in oil spilt at sea. Oil Chem. Pollut. 4, 311–328.
Cochran, R., Scott, P., 1971. The growth of oil slicks and their controls by surface chemical agents. J. Pet. Technol., 781–787.

Cretney, W.J., Macdonald, R.W., Wong, C.S., Green, D.R., Whitehouse, B., Greesey, G.G., 1981. Biodegradation of a chemically dispersed crude oil. Proceedings of 1981 Oil Spill Conference, March 29–April 5, Atlanta, USA, pp. 37–43.

Delvigne, G.A.L., 1993. Natural dispersion of oil by different sources of turbulence. Proceedings of 1993 Oil Spill Conference, Atlanta, USA, pp. 415–419.

Delvigne, G.A.L., Sweeney, C.E., 1988. Natural dispersion of oil. Oil Chem. Pollut. 4, 281–310.

Dietrich, D.E., 1997. Application of a modified "a" grid ocean model having reduced numerical dispersion to the Gulf of Mexico circulation. Dyn. Atmos. Oceans 27, 201–217.

Elliott, A.J., 1986. Shear diffusion and the spread of oil on a water surface of the North Sea. Deutsche. Hydrogr. Zeitschrift 39 (3), 113–137

Elliott, A.J., Jones, B., 2000. The need for operation forecasting during spill response. Mar. Pollut. Bull. 40 (2), 110–121.



- Feng, S., Reed, M., French, D.P., 1989. The chemical database for natural resource damage assessment model system. Oil Chem. Pollut. 5, 165–193.
- Genders, S., 1988. In situ detection and tracking of oil in the water column. Oil Chem. Pollut. 4, 113–126.
- Hunter, J.R., 1987. The application of Lagrangian particle-tracking technique to modeling of dispersion in the sea. In: Noye, J. (Ed.), Numercal Modeling: Applications for Marine Systems, North Holland, pp. 257–269.
- Johansen, O., 1987. DOOSIM A new simulation model for oil spil management. 1987 Oil Conference, Paper 169 (preprint).
- Ibraev, I.R., Ozsoy, E., Ametistova, L.E., Sarkisyan, A.S., Sur, H.I., 1998. Seasonal variability of the Caspian Sea dynamics: barotropic motion driven by climatic wind stress and Volga River discharge. Abstracts of Konstantin Fedorov Memorial Symposium, Sankt-Petersburg, Pushkin, St. Petersburg, 18–22 May, 1998, p. 65.
- Ikonnikova, L.N., 1960. Calculations of waves in the Caspian Sea and winds over it. Trudy GOIN 50 (in Russian).
- Klevtsova, N.D., 1966. Sea surface currents in the middle and south parts of the Caspian Sea under different wind fields. Oceanology 6 (1), 82–88 (in Russian).
- Klevtsova, N.D., 1967. Sea current regime near east coast of the middle and south Caspian basins. Proceedings of of Hydrometeoobservatory of Baku. Baku, vol. 3, pp. 44–49 (in Russian).
- Kolpack, R.L., Plutchak, N.B., Stearns, R.W., 1977. Fate of oil in water environment Phase II, a dynamic model of the mass balance for released oil. Publication 4313, American Petroleum Institute, Washington, DC.
- Korotenko, K.A., 1992. Modeling turbulent transport of matter in the ocean surface layer. Oceanology 32 (1), 5–13.
- Korotenko, K.A., 1994a. The random walk concept in modeling matter transport and dispersion in the Sea. J. Moscow Phys. Soc., vol. 4 (4), Allerton Press, NY, pp. 335–338.
- Korotenko, K.A., 1994b. On the formation of mesoscale anomalies of the matter concentration field in ocean local upwelling zone regions. Oceanology 34 (3), 330–338.
- Korotenko, K.A., Mamedov, R.M., 2000. 3-D flow/particle model for prediction matter transport in the sea: Modelling oil pollution in the Caspian Sea. Physics and Chemistry of the Earth, Elsevier Science, in press.
- Korotenko, K.A., Mamedov, R.M., 2001. Modeling of oil slick transport processes in coastal zone of the Caspian Sea. Oceanology 41 (1) 37–48.
- Kosarev, A.N., 1970. Pecularities of thermal anomaly at eastern coast of the middle part of Caspian Sea. Complex stud. Caspian Sea 1, 197–211.
- Kosarev, A.N., 1990. The Caspian Sea. Structure and Water Dynamics. Nauka, Moscow (in Russian).
- Ledney, V.A., 1943. Currents of the Northern and Central parts of the Caspian Sea. Moscow, p. 128 (in Russian).
- Li, M., Garret, C., 1998. The relationship between oil droplet size and upper ocean turbulence. Mar. Pollut. Bull. 36, 961–970.
- Mackay, D., Bouist, I., Mascarenhas, R., Paterson, S., 1979. Oil spill processes and models. Publication EE-88, Report for Fisheries and Environmental Canada, Ottawa, Ontario, pp. 120.
- Mackay, D., Matsugu, R., 1973. Evaporation rate of liquid hydrocarbon spills on land and water. Can. J. Chem. Engng. 51 434-439
- Mackay, D., McAuliffe, C., 1988. Fate of hydrocarbons discharged at sea. Oil Chem. Poll. 5, 1–20.
- Mackay, D., Stiver, W., Tebeau, P.A., 1983. Testing of crude oil and petroleum products for environmental purposes. Proceedings of 1983 Oil Spill Conference, American Petroleum Institute, Washington, DC, pp. 331–337.

- McAuliffe, C.D., 1986. Organism exposure to volatile hydrocarbons from untreated and chemically dispersed crude oils in field and laboratory. Proceedings of the 9th Arctic Marine Oilspill Program Technical Seminar, Environment Canada, Beuuregard press, Ottawa, Canada, pp. 497–526.
- Mellor, G.L., Yamada, T., 1982. Development of a turbulence closure model for geophysical fluid problems. Rev. Geophys. Space Phys. 20, 851–875.
- Monin, A.S., Yaglom, A.M., 1965. Statistical Hydromechanics. Part I, Nauka, Moscow, p. 640.
- Moore, S.F., Dwyer, R.L., Datz, A.M., 1973. A preliminary assessment of the environmental vulnerability of Michias Bay, Main to oil supertankers. Rep. no. 162, Dept. of Civil Engng. M I T
- Ozmidov, R.V., Korotenko, K.A., 1989. Investigations of diffusion processes in the coastal zone of the Black Sea, Moscow, p. 174 (in Russian).
- Price, J.F., Weller, R.A., Pinkel, R., 1986. Diurnal cycling: Observations and models of the upper ocean response to diurnal heating, cooling, and wind mixing. J. Geophys. Res. 91 (C7), 8411–8427.
- Proctor, R., Flather, R.A., Elliot, A.J., 1994. Modeling tides and surface drift in the Atabian Gulf-application to the Gulf Spill. Cont. Shelf Res. 14 (5), 531–545.
- Reed, M., 1989. The physical fates component of natural resource damage assessment model system. Oil Chem. Poll. 5, 99–123.
- Reed, M., Gundlach, E., Kana, T.A., 1989. Coastal zone spill model: development and sensitivity studies. Oil Chem. Poll. 5, 441–449.
- Reed, M., Johansen, O., Brandvik, J., Daling, S., Lewis, A., Fiocco, R., Mackay, D., Prentki, R., 1999. Oil spill modeling the close of the 20th century: overiew of the state of the art. Spill Sci. Technol. Bull. 5 (1), 3–16.
- Reijnard, R., Rose, R., 1982. Evaporation of crude oil at Sea. Water Res. 16, 1319–1325.
- Sebastiao, P., Soares, C.G., 1998. Weathering of oil spills for oil components. In: Garsia-Martinez. R., Brebbia, C.A. (Eds). Oil and Hydrocarbon Spills. Modeling Analysis and Computing. Computation Mechanics Publications, Southampton UK, pp. 63-72
- Sorstrom, S.E., 1987. The 1985 full scale experimental oil spill at Haltenbanken, Norway. Oil Chem. Poll. 3, 455–469.
- Spaulding, M.L., Saila, S.B., Reed, M., Lorda, E., Walker, H., Isaji, T., Swanson, J., Anderson, E., 1988. Assessing the impact of oil spills on a commercial fishery. Final Report to minerals management Service. Contract no. AA851-CTO-75. NTIS no. PB83-149104.
- Spaulding, M.L., 1988. A state-of-art review of oil spill trajectory and fate modeling. Oil Chem. Poll. 4, 39–55.
- Spaulding, M.L., 1995. Oil pill and fate modeling: State-ofart review. Presented at the Second International Oil Research and Development Forum, 23–26 May, IMO, London, UK, 1995.
- Thorpe, S.A., 1995. Vertical dispersion of oil droplets in strong winds; the Brayer oil spill. Mar. Pollut. Bull. 30, 756–758.
- Tuzhilkin, V.S., Kosarev, A.N., Trukhchev, D.I., Ivanova, D.P., 1997. Seasonal features of general circulation in the Caspian deep water part. Meteorology and Hydrology 1, 91–99 (in Russian).
- Varlamov, S.M., Yoon, J.-H., Hirose, N., Kawamura, H., 1998. In: Garsia-Martinez, R., Brebbia, C.A. (Eds.), Oil and Hydrocarbon Spills. Modeling Analysis and Computing. Computation Mechanics Publications, Southampton UK, pp. 359–369.
- Yang, W.C., Wang, H., 1977. Modeling of oil evaporation in aqueous environment. Water Res. 11, 879–887.